AAPS PharmSciTech, Vol. 14, No. 2, June 2013 (© 2013)
DOI: 10.1208/s12249-013-9940-6

Research Article

Concomitant Pseudopolymorphs of 10-Deacetyl Baccatin III

Lakshmi Kumar Tatini,[1,3] N. Someswara Rao,[1,2] Muzaffar Khan,[1] Krishna Sumanth Peraka,[1] and K. V. S. R. Krishna Reddy[1]

Received 14 June 2012; accepted 22 February 2013; published online 13 March 2013

Abstract. Three new solvates [mono-dimethyl sulfoxide (mono-DMSO), mono-dimethyl acetamide (mono-DMA) and mono-dimethyl formamide (mono-DMF)] of 10-Deacetyl baccatin III, were generated by slow evaporation in DMSO, DMF, and DMSO/DMA (1:1) solvent systems respectively. Two concomitant forms mono-DMSO(a new form) and di-DMSO (a known form) were obtained in the DMSO solvent system. Yet two other concomitant forms mono-DMA (a new form) and di-DMSO (a known form) were obtained in DMSO/DMA (1:1) solvent system. A fourth solvate mono-DMF (a new form) was crystallized in unimolar ratio using DMF as a solvent. These solvates were characterized using powder X-ray diffraction, differential scanning calorimeter, thermogravimetric analysis (TGA), and spectroscopic [^{13}C solid-state nuclear magnetic spectroscopy, solution ^{1}H NMR, and Fourier transform infrared] techniques. The interactions between host and guest molecules were elucitated by single-crystal X-ray diffraction data. In all the cases, guest molecules are connected to the host molecules by O–H···O hydrogen bonds. A remarkable difference in the desolvation onset temperatures of di- and mono-DMSO solvates was observed which was also featured by a corresponding weight loss during TGA analysis.

KEY WORDS: 10-deacetyl baccatin III; concomitant; pseudopolymorphs; solid-state characterization.

INTRODUCTION

In general, the discovery of inclusion compounds is a result of serendipity, obtained during crystallization from various solvents (1). However, development in supramolecular chemistry (2) and crystal engineering reveals that host–guest compounds can be rationally designed and synthesized. Desiraju has more aptly defined crystal engineering as "the understanding of intermolecular interactions in the context of crystal packing and in the utilization of such understanding in the design of new solids with desired physical and chemical properties" (3). By understanding the history of molecular arrangements in crystals, host–guest pioneers described how to design novel host materials (4–8). The host–guest, inclusion compounds and solvates of the latter case have been called as pseudopolymorphs (9,10). The study of inclusion compounds is one of the hot topics in chemical research (11–19) since it has applications in magnetism, gas storage devices, nonlinear optical materials, targeted drug delivery, *etc.* (19,20).

The formation of two different forms of a same species simultaneously in the same container under identical conditions is termed as "concomitant polymorphs" or "concomitant pseudopolymorphs" (21). The situations in which polymorphs concomitantly crystallize are determined by the experimental conditions in relation to both the free energy–temperature relationships and the relative kinetic factors. The possibilities of concomitant pseudopolymorphs was explained by Dinabandhu Das *et al.*, when a host (H) is crystallized from a solvent (S), either only one kind of solvate (H.nS) could be formed, or different solvates such as H.n1S, H.n2S, *etc.* can result depending on the stoichiometry of H and S (22). In principle, there are four possible structural outcomes of crystallizing H (host) from a binary mixture of solvents S1 and S2: (1) the host can crystallize in its apohost form (without solvent); (2) H can include only solvent S1 to form H.n1S1; (3) H can include only solvent S2 to form H.n2S2 and (4) both solvents can be included to yield a so-called "mixed solvate (23,24)" H.n1S1.n2S2, mixed crystal solvates are generally not observed. Concomitant pseudopolymorphs have recently been investigated in a systematic manner (9,10,22). Though, dual concomitant pseudopolymorphs occur frequently in a

Electronic supplementary information available: CCDC reference numbers 863865–863866

[1] Analytical Development, Aptuit Laurus Pvt. Ltd, ICICI Knowledge Park, Turkapally, Shameerpet, Hyderabad 500078, India.
[2] Department of Inorganic and Analytical Chemistry, Andhra University, Visakhapatnam 530003, India.
[3] To whom correspondence should be addressed. (e-mail: kumarltatini@gmail.com)

mixture of solvents in unimolar ratios, concomitant polymorphs of one host and two guests, one host and one guest are not very common. We have reported such rare case of concomitant crystallization of 10-DAB III, a pharmaceutically relevant compound in different stoichiometric solvates using DMSO and a mixture of DMSO and DMA.

10-DAB III ((2a*R*,4*S*,4a*S*,6*R*,9*S*,11*S*,12*S*,12a*R*,12b*S*)-12b-(acetyloxy)-12-(benzoyloxy)-1,2a,3,4,4a,6,9,10,11,12,12a,12b-dodecahydro-4,6,9,11-tetrahydroxy-4a,8,13,13-tetramethyl-7,11-methano-5H-cyclodeca(3,4)benz(1,2-b) oxet-5-one) (Scheme 1) is closely related to natural organic compound isolated from the Pacific yew tree (*Taxus brevifolia*) and related species. 10-DAB III is a key starting material of paclitaxel (Tazol) and docetaxel (Taxotere) which are used as anticancer drugs. Both paclitaxel and docetaxel possess a common tetracyclic ring and differ only in the substitution of side chains.

So far, only one crystal structure of 10-DAB III was reported in Cambridge Crystallographic Data Centre (CCDC), a dimethyl sulfoxide (DMSO) solvate in 1:2 ratio (**Form III**) (25). In the present study, we have crystallized three new solvates of 10-DAB III *viz*. mono-DMSO (**Form I**), mono-DMA (**Form II**), and mono-DMF (**Form IV**). All these forms of 10-DAB III including Form **III** were fully characterized by powder X-ray diffraction (PXRD), NMR (solid state and solution state), Fourier transform infrared (FT-IR), differential scanning calorimeter (DSC), and thermogravimetric analysis (TGA) techniques. Single-crystal X-ray diffraction (SXRD) studies were performed on Form **I** and **II** to elucidate the interaction between host and guest molecules in the crystal packing system. The Form **IV** crystallized as very thin crystals and therefore was not deemed suitable for SXRD analysis.

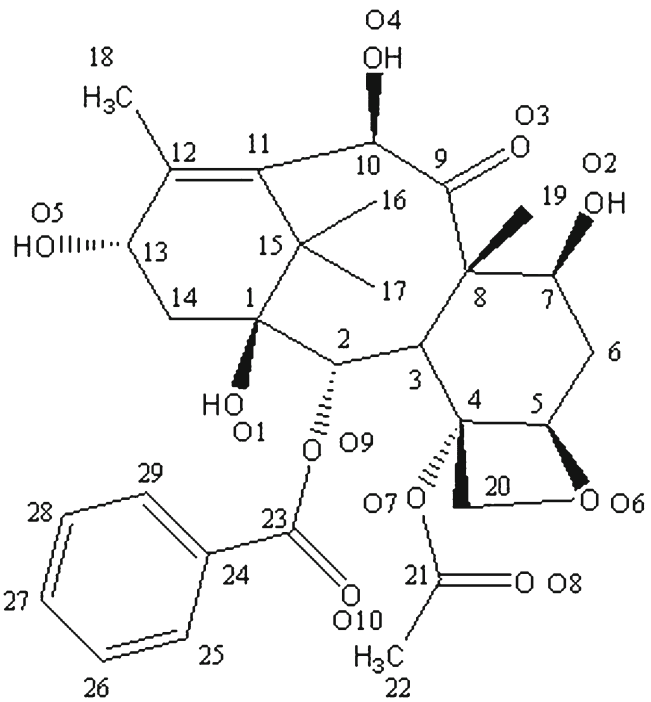

Scheme 1. Structure of 10-DAB III

MATERIALS AND METHODS

Materials

10-DAB III (M.Wt—544, $C_{29}H_{36}O_{10}$) was procured from Deccan Nutraceuticals private limited, Pune, India. GC-grade solvents DMSO, DMA and DMF were procured from Merck Chemicals, Darmstadt, Germany.

Preparation of 10-DAB III Solvates

Forms **I** and **III** were crystallized from a supersaturated solution of 10-DAB III. An excess amount of 10-DAB III was dissolved in DMSO at 60°C and the solution was filtered through 0.45 μm Whatman filter. The filtered solution was allowed to evaporate slowly at room temperature and after 6 days of evaporation, crystals with two different morphologies having diamond and plate shapes were observed (Fig. 1). These crystals were separated manually and dried.

Forms **II** and **III** were crystallized from a supersaturated solution of 10-DAB III by dissolving its excess amount in equal volumes of DMA and DMSO at 60°C. The solution was filtered through 0.45 μm Whatman filter and allowed to evaporate slowly at room temperature. After 8 days, crystals with two different morphologies having needle and diamond shapes were observed (Fig. 2). These crystals were separated manually and dried.

Form **IV** was crystallized from a saturated solution of 10-DAB III in DMF at 40°C and allowed to evaporate slowly at room temperature. After 15 days of evaporation, very thin crystals were obtained at the bottom of the conical flask. The crystals were filtered through the Buchner funnel and dried.

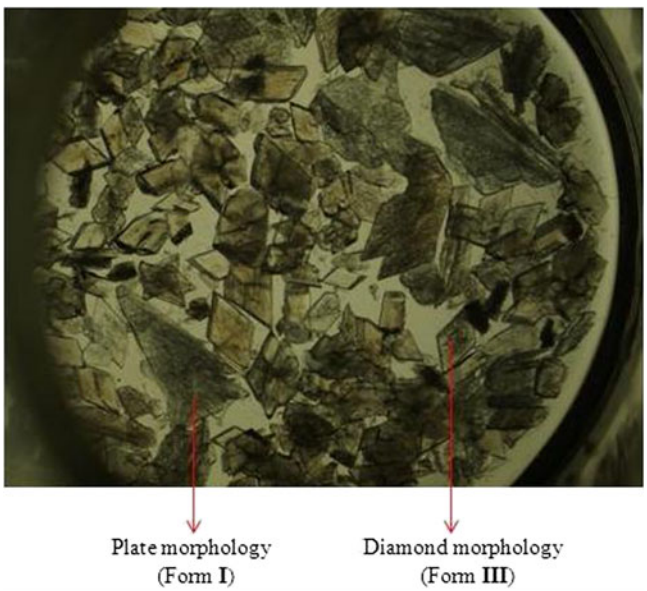

Fig. 1. Photomicrograph of concomitant solvates of 10-DAB III (Forms **I** and **III**)

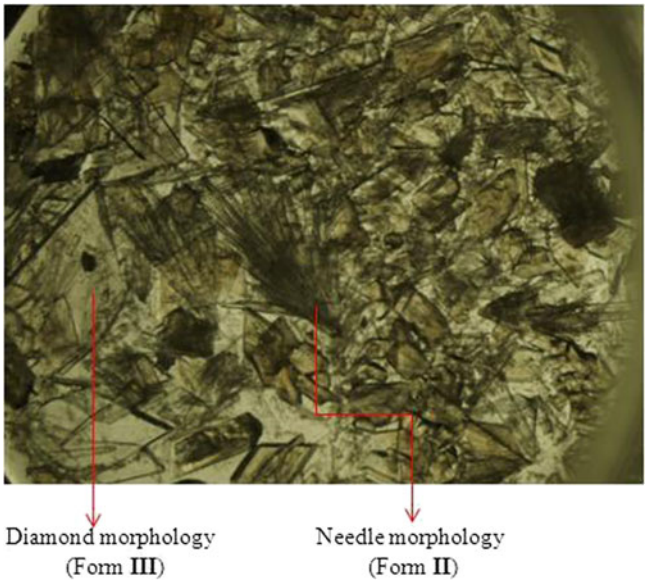

Fig. 2. Photomicrograph of concomitant solvates of 10-DAB III (Forms **II** and **III**)

Methods

SXRD

X-ray reflections of Forms **I** and **II** were collected on an Oxford Xcalibur Gemini Eos CCD diffractometer using Mo-Kα, radiation. Data reduction was performed using CrysAlisPro (version 1.171.33.55). OLEX2-1.0 (26) and SHELX-TL 97 were used to solve and refine the data. All non-hydrogen atoms were refined anisotropically and C–H hydrogens were fixed. The O–H hydrogens were located from the differences in electron density maps and C–H hydrogens were fixed.

Powder X-Ray Diffractometry

PXRD patterns were recorded using a Rigaku MiniFlex (Tokyo, Japan) powder diffraction system, equipped with a horizontal goniometer in the $\theta/2\theta$ mode. The X-ray source was nickel-filtered Kα emission of copper (1.54056 Å). Samples were packed into a glass holder and were scanned over the range of 3 to 45° 2θ, at a scan rate of 2.0 2θ/min.

Thermal Analysis

Thermogravimetric analysis was performed on the samples using a TA Q 500 series (TA Instruments, Newcastle, DE, USA) using Q-Advance software. Approximately 4–8 mg of sample was weighed into a platinum pan and heated in a typical temperature range of 30–250°C. Two-point calibration of the temperature was performed with ferromagnetic materials (Ni, Curie-point standards, TA instruments). Heating rates of 10°C/min were applied and dry nitrogen was used as a purge gas (sample purge: 60 mL/min and balance purge: 40 mL/min).

Differential Scanning Calorimetry (DSC) was performed using a TA Q 200 series (TA Instruments, Newcastle, DE, USA) operated through Q-Advance software. Approximately 2–4 mg of sample (solid forms) was placed into a Tzero aluminum pan. The pan was covered with a lid and then crimped. The sample cell was heated under nitrogen purge (50 mL/min) at a rate of 10°C/min, from 50°C up to a temperature of 270°C. Indium metal (TA instruments) was used as the calibration standard. Reported temperatures are the onset temperatures.

Spectroscopy

FT-IR spectra were recorded using FT-IR spectrometer (PerkinElmer, USA) equipped with Spectrum-100 analyzing software. Potassium bromide (spectroscopy grade) (Merck, Darmstadt, Germany) disk pelletization method was employed for sample preparation. The pellets were prepared by mixing of the sample with potassium bromide (1:100) in a mortar and compressed at a pressure of 6 to 8 bar. Each spectrum was derived from 16 single averaged scans collected in the mid IR region of 400–4,000 cm^{-1} at a spectral resolution of 2.0 cm^{-1}.

The spectrometer was equipped with a solid-state probe, cross-polarization magic angle spinning (CP/MAS-II) and ^{13}C Solid State Nuclear Magnetic Spectroscopy (^{13}C SSNMR) spectra were recorded with Bruker Avance-II 75 MHz spectrometer (Bruker, Switzerland) with TOPSPIN version 2.0 software. The static field of the superconducting magnet was 7.05 T and cross-polarization total suppression of spinning side bands (CP/TOSS) pulse sequence was used to perform the experiments. The instrument was operated at a spinning rate of 5 KHz. The cross polarization magic angle and ^{13}C signal were optimized using KBr and glycine as standards, respectively.

Solution ^{1}H-NMR spectra were acquired at ambient temperature on a Bruker Avance-II 300 MHz spectrometer at a ^{1}H Larmor frequency of 300.131 MHz and DMSO-d_6 was used as a solvent. The spectrum was acquired with a ^{1}H pulse width of 10.50 μs, a 3.64-s acquisition time, a 5-s delay between scans, a spectral width of 15 ppm and 32 co-added scans. The free induction decay was processed using TOPSPIN version 2.0 software and an exponential line broadening factor of 0.2 Hz to improve the signal-to-noise ratio.

RESULTS AND DISCUSSION

Crystal Structure Analysis by SXRD

Form **I** crystallized as plate morphs in the monoclinic crystal system (space group $P2_1$) with one molecule each of 10-DAB III and dimethyl sulfoxide in the asymmetric unit (Table I). O–H···O hydrogen bond (Table II) between the host molecules (O1–H1···O8, 2.14, 146; O2–H2A···O6, 2.00, 170 and O4–H4···O10, 2.32, 158.1) form two adjacent ring motifs $R_3^3(25)$, and $R_3^3(21)$ (Fig. 3). Guest molecules are connected to the host molecules by O–H···O11 hydrogen bond (O5–H5A···O11, 1.99, 172). The O4–H4 hydroxyl

Table I. Crystallographic Parameters of Forms **I**, **II**, and **III**

	I	II	III CSD Ref Code:WOVSAB
Empirical formula	$C_{29}H_{36}O_{10}\cdot C_2H_6OS$	$C_{29}H_{36}O_{10}\cdot C_4H_9NO$	$C_{29}H_{36}O_{10}\cdot 2C_2H_6OS$
Formula weight	622.71	631.70	700.83
Crystal system	Monoclinic	Monoclinic	Monoclinic
Space group	$P2_1$	$C2$	$P2_1$
T (K)	298	298	293
a/Å	8.5605(8)	42.066(7)	9.3677(10)
b/Å	13.4700(11)	8.5246(10)	21.991(4)
c/Å	13.6383(11)	9.2940(13)	9.4564(11)
α/°	90.00	90.00	90.00
β/°	100.284(8)	100.959(14)	115.827(9)
γ/°	90.00	90.00	90.00
V/Å^3	1547.4(2)	3272.0(8)	1753.5(4)
D_{calcd}(gcm^{-3})	1.337	1.282	1.327
μ(mm^{-1})	0.164	0.096	0.213
Z/Z′	1/2	1/4	1/2
Reflns collected	11537	6633	4342
Unique reflns	6306	3940	4103
Observed reflns	3785	5234	3005
R_1 [I > 2 σ(I)]	0.0575	0.0495	0.056
wR_2 (all)	0.0774	0.0983	0.136
Goodness-of-fit	0.995	1.034	–
Size of crystal (mm^3)	0.34×0.30×0.24	0.42×0.32×0.30	0.5×0.4×0.3

groups do not participate in any intermolecular hydrogen bonding.

Form **II** crystallized as needles in the monoclinic crystal system (space group $C2$) with one molecule of

Table II. Hydrogen Bond Geometries in Crystal Structures of Form **I** and **II**

Interactions	H···A/ Å	D···A/ Å	∠D–H···A/º	Symmetry code
Form I				
O(1)–H(1)···O(8)	2.14	2.862	146	−1 + *x*,*y*,*z*
O(2)–H(2A)···O(6)	2.00	2.816	170	1−*x*,−1/2 + *y*,−*z*
O(4)–H(4)···O(3)	2.18	2.615	113	Intramolecular
O(4)–H(4)···O(10)	2.32	3.093	158	−*x*,−1/2 + *y*,−*z*
O(5)–H(5A)···O(11)	1.99	2.808	172	1−*x*,1/2 + *y*,1−*z*
C(2)–H(2)···O(10)	2.31	2.739	106	Intramolecular
C(3)–H(3)···O(8)	2.53	3.093	116	Intramolecular
C(5)–H(5)···O(10)	2.49	3.441	163	1 + *x*,*y*,*z*
C(14)–H(14B)···O(9)	2.44	2.882	107	Intramolecular
C(16)–H(16B)···O(4)	2.55	3.161	122	Intramolecular
C(16)–H(16C)···O(3)	2.51	3.082	119	Intramolecular
C(17)–H(17C)···O(1)	2.56	2.918	102	Intramolecular
C(19)–H(19A)···O(6)	2.45	3.312	149	Intramolecular
C(26)–H(26)···O(5)	2.52	3.266	137	1−*x*,1/2 + *y*,1−*z*
C(29)–H(29)···O(3)	2.56	3.198	126	−*x*,1/2 + *y*,−*z*
Form II				
O(1)–H(1)···O(8)	2.15	2.892	150	*x*,−1+*y*,*z*
O(2)–H(2)···O(11)	1.83	2.627	165	–
O(4)–H(4)···O(3)	2.07	2.571	119	Intramolecular
O(5)–H(5)···O(2)	1.98	2.800	173	*x*,*y*,1 + *z*
C(2)–H(2A)···O(10)	2.24	2.694	107	Intramolecular
C(3)–H(3)···O(8)	2.50	3.076	117	Intramolecular
C(5)–H(5A)···O(10)	2.43	3.368	160	*x*,1 + *y*,*z*
C(14)–H(14A)···O(9)	2.54	2.945	105	Intramolecular
C(17)–H(17A)···O(3)	2.58	3.196	122	Intramolecular
C(17)–H(17C)···O(4)	2.56	3.135	119	Intramolecular
C(19)–H(19B)···O(6)	2.43	3.287	148	Intramolecular
C(31)–H(31C)···O(3)	2.58	3.454	151	*x*,1 + *y*,*z*

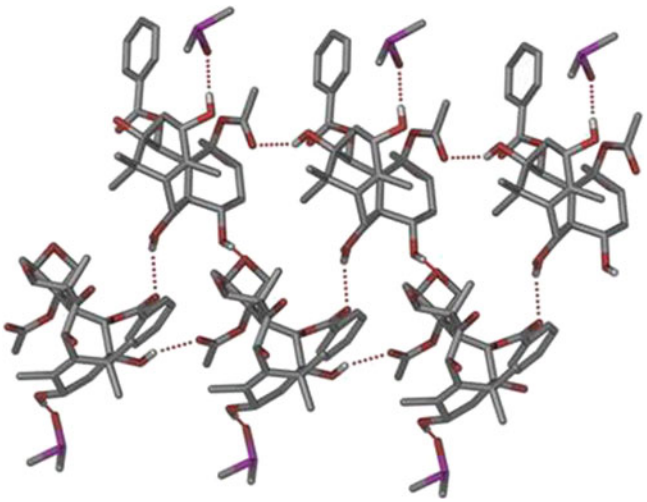

Fig. 3. Ring motif $R_3^3(25)$, and $R_3^3(21)$ of the host molecule of Form **I**. Guest molecules are connected by O–H···O hydrogen bond

each of 10-DAB III and dimethyl acetamide in the asymmetric unit (Table I). The O–H···O hydrogen bond (Table II) is the structure governing interaction although several auxiliary C–H···O hydrogen bonds are also present in the crystal structure. The O–H···O hydrogen bonding between the host molecules (O5—H5···O2, 1.98 Å, 173° and O1—H1···O8, 2.15 Å, 150°) form a ring motif $R_4^4(34)$ (Fig. 4a). DMA molecules are connected to 10-DAB III molecules *via* O–H···O hydrogen bond (O2–H2···O11, 1.83 Å, 165°) as shown in Fig. 4b. The DMA molecules are interconnected by very weak C–H···O single hydrogen bonds (C32–H32A···O11, 2.78, 117) to form a zigzag chain along C2 axis (Fig. 4c). Unlike in Form **I**, the O4–H4 hydroxyl groups do not participate in any intermolecular hydrogen bonding. Another contrasting feature is that there is no interaction between the guest molecules as observed in Form **I**. The conformational differences are shown in Fig. 5.

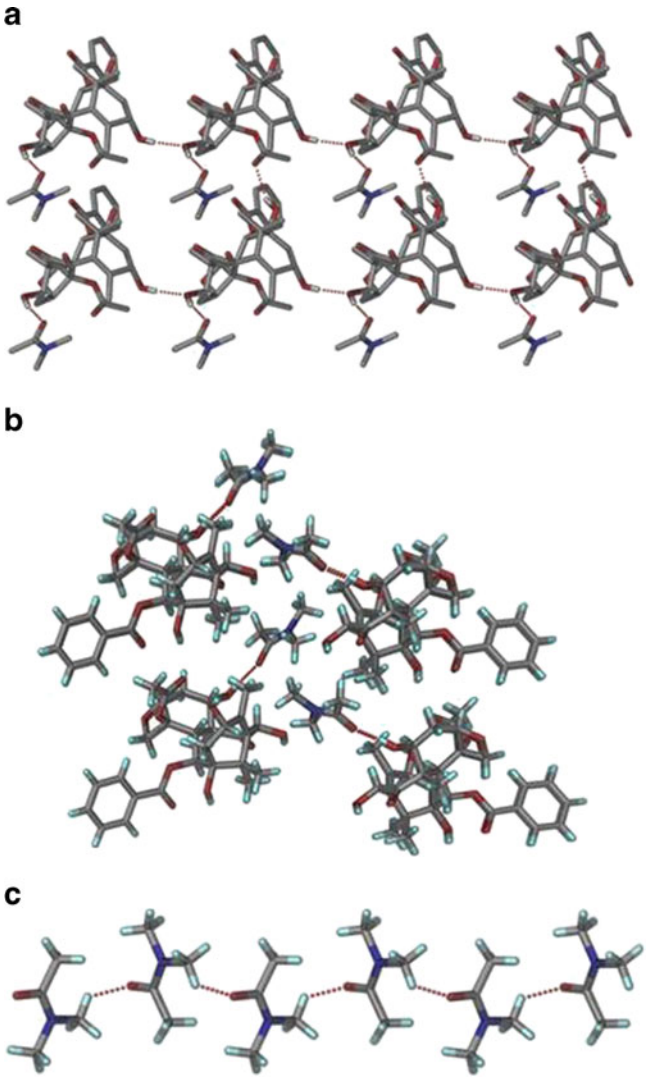

Fig. 4. **a** O–H···O hydrogen bond forms the ring motif $R_4^4(34)$. **b** 10-DAB III molecules are connected DMA *via* O—H···O hydrogen bond. **c** Zig zag chains of DMA molecules connected by C–H···O hydrogen bond along C2 rotation axis

PXRD

The crystals of 10-DAB III solvates were gently ground in a mortar pestle and the powdered samples were analyzed by PXRD. The PXRD patterns of all the solvated forms of 10-DAB III are shown in Fig. 6a. The distinct patterns show that the solvates posses different crystal structures. The following characteristic 2θ peak positions can be used to discriminate the solid forms. Form **I**: 6.66, 9.32, 12.44, 13.26, 14.74, 16.78, 16.86, 19.92, 20.92, 21.80, 23.90, 24.12, and 27.48° 2θ; **II**: 4.16, 8.40, 9.58, 14.48, 17.90, 19.02, 19.48, 21.10, 21.70, 22.34, and 22.66° 2θ; **III**: 8.00, 10.30, 11.08, 11.22, 13.66, 16.06, 16.34, 19.18, 19.44, 20.56, 21.12, 22.40, 22.50 and 21.14° 2θ;**IV**: 6.40, 9.10, 12.96, 13.14, 14.44, 14.70, 16.48, 16.74, 19.18, 20.42, 23.66, 24.86, and 27.00° 2θ. The experimental PXRD patters of Form **I**, **II**, and **III** were compared with the simulated patterns from the single-crystal diffraction structures. Figure 6b–d shows excellent agreement between experimental and simulated patterns for the three solvates.

TGA

The data on weight loss obtained by thermogravimetric analysis was evaluated for determining the solvent to solute ratios of the solvated forms of 10-DAB III. The experimental results of thermogravimetric analysis are tabulated in Table III and the thermograms of 10-DAB III with its corresponding solvate are presented in Fig. 7.

1. Forms **I** and **III**
   The TGA curve of $DAB_{M\text{-}DMSO}$ represent weight loss beginning at about 91°C probably due to the loss of solvent. The weight loss obtained for Forms **I** and **III** are about 12.8% and 21.6%, respectively. This loss in weight can be correlated to a stoichiometric release of 1.02 and 1.94 mol of DMSO. Thus, it can be inferred from the TGA data that 10-DAB III accommodates DMSO solvent in a 1:1 and 1:2 stoichiometric molar ratios in Forms **I** and **III**, respectively.

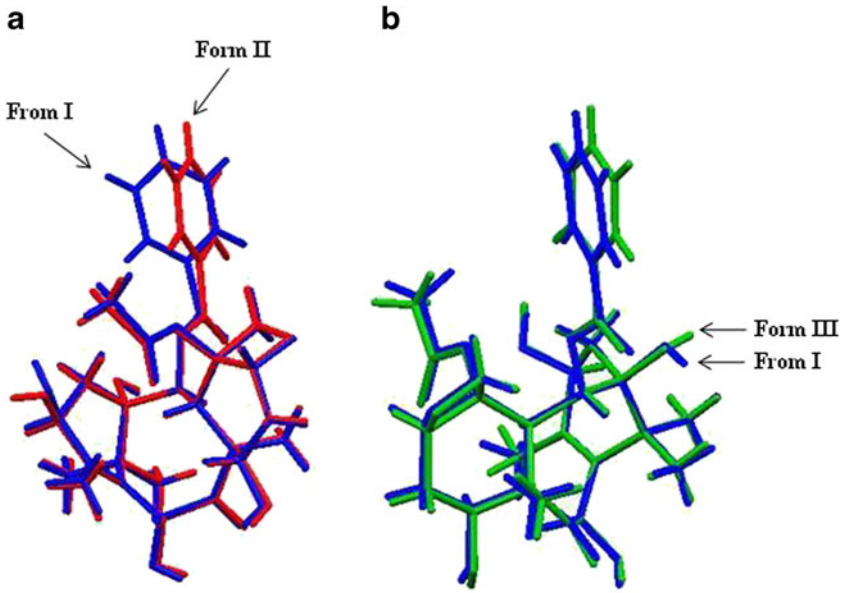

Fig. 5. Overlay diagram showing the differences in conformation of **a** O–H groups of C13 and benzoate group. **b** O–H directions of C1

2. Form **II**
From TGA analysis, the weight loss observed for DAB_{DMA} was 12.9% at about 74°C. This weight loss corresponds to 0.94 mol of DMA solvent. Thus, it can be concluded that the 10-DAB III can accommodate DMA solvent in a 1:1 stoichiometric molar ratio in Form **II**.

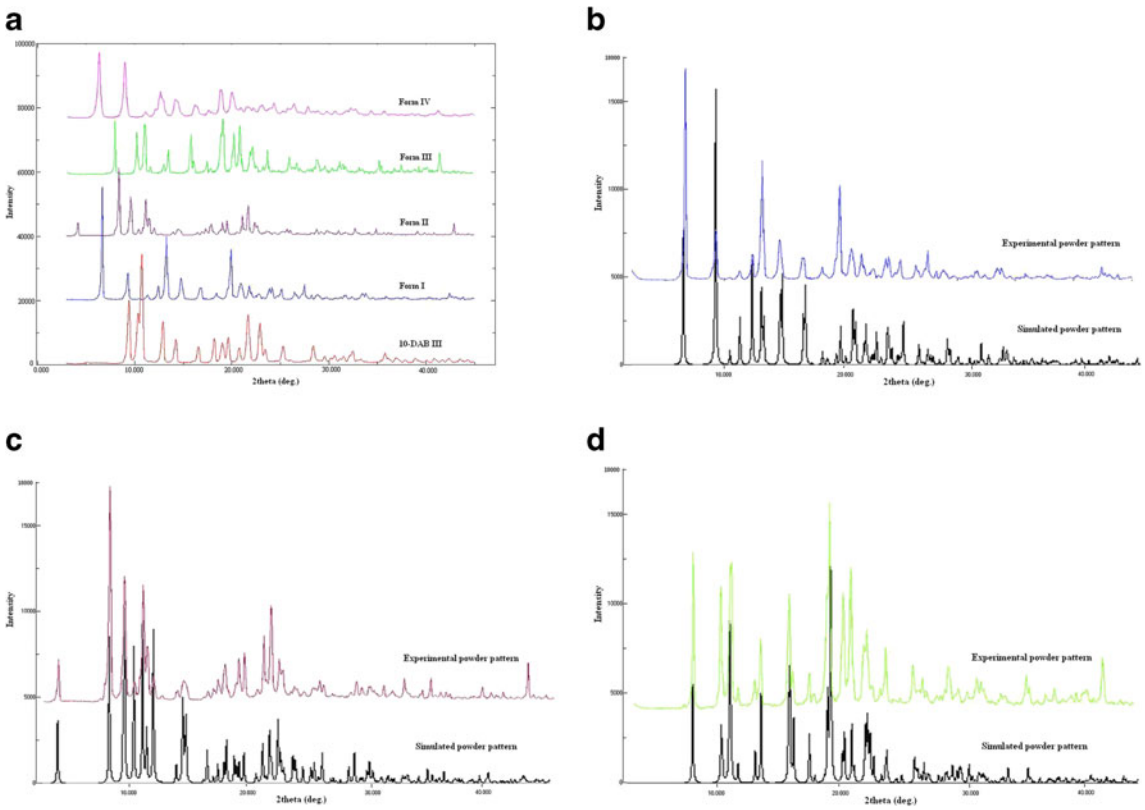

Fig. 6. **a** Overlaid PXRD diffractograms of 10-DAB III and its solid forms. **b** Overlay of simulated and experimental powder patterns of Form **I**. **c** Overlay of simulated and experimental powder patterns of Form **II**. **d** Overlay of simulated and experimental powder patterns of Form **III**

Table III. Comparison of the DSC and TGA Data of 10-DAB III and its Solid Forms

Compound	Endotherm (°C)[a]	ΔH (J/g)	Endotherm (°C)[b]	ΔH (J/g)	Weight loss (%)	
					Experimental	Expected
10-DAB III	–	–	247.97	54.51	–	–
Form **I**	129.86	35.54	246.01	50.99	12.84	12.54
Form **II**	138.60	102.80	252.67	56.33	12.92	13.80
Form **III**	166.05	93.77	248.20	57.20	21.60	22.28
Form **IV**	115.70	102.40	249.36	57.29	11.46	11.83

[a] Endotherms correspond to loss of solvent
[b] Endotherms correspond to onset temperature of solid forms

3. Form **IV**
   From TGA analysis, the weight loss observed for DAB_{DMF} was 11.5% at about 92°C. This weight loss corresponds to 0.97 mol of DMF solvent. Thus, it can be concluded that the 10-DAB III can accommodate DMF solvent in a 1:1 stoichiometric molar ratio in Form **IV**.

In Table III, a comparison has been made between the theoretical weight loss and the experimental weight loss from TGA data. From Table III, it can be seen that there is a good agreement between the experimental and theoretical weight loss, indicating that the solvent molecules exist in stoichiometric ratios within the crystal lattices.

DSC

DSC thermograms of 10-DAB III and its solid forms are shown in Fig. 8 and the onset temperatures and its enthalpies are tabulated in Table III. All the four forms exhibit two endotherms, the first broad endotherm obtained in each form can be attributed to the desolvation while the second endotherm at a much higher temperature corresponds to the melting with decomposition.

On comparing the results obtained from the DSC data of Forms **I** and **III**, distinct differences are observed in onset temperature as well as enthalpy; even though these two forms are crystallized from the same solvent, DMSO. In Forms **I** and **III**, the onset temperatures of first endotherm are at 129.9°C and 166.1°C, respectively. Similarly, the enthalpies of Forms **I** and **III** calculated from the first endotherm are 35.5 and 93.8 J/g, respectively. The differences in the onset temperatures and the enthalpies for the two forms are probably due to the different affinities of the solvent towards the solute. It can be inferred from the onset temperature and the enthalpy that DMSO is weakly bound to 10-DAB III in Form **I**, whereas DMSO solvent is strongly bound to 10-DAB III in Form **III**. This also indicates that there is a probable difference in the crystal packing of the two forms.

In the case of Forms **II** and **IV** observed onset temperatures of first endotherm at 138.6°C and 115.7°C, respectively. After desolvation, all the four solvates are found to melt at about 249°C, which in turn correspond to the melting temperature of 10-DAB III. Based on the above results, it can be concluded that after desolvation of all the forms are converted into a most stable form of 10-DAB III.

FT-IR

FT-IR spectroscopy has been successfully used for exploring the differences in molecular conformations, crystal packing and hydrogen bonding arrangements for

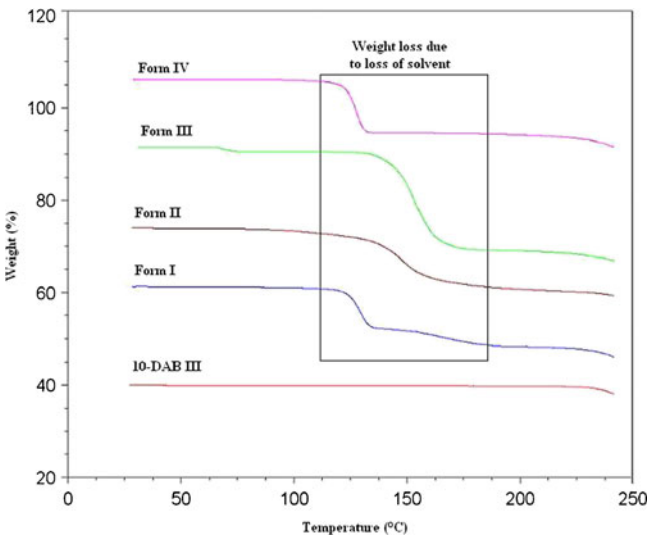

Fig. 7. TGA thermograms of 10-DAB III and its solid forms

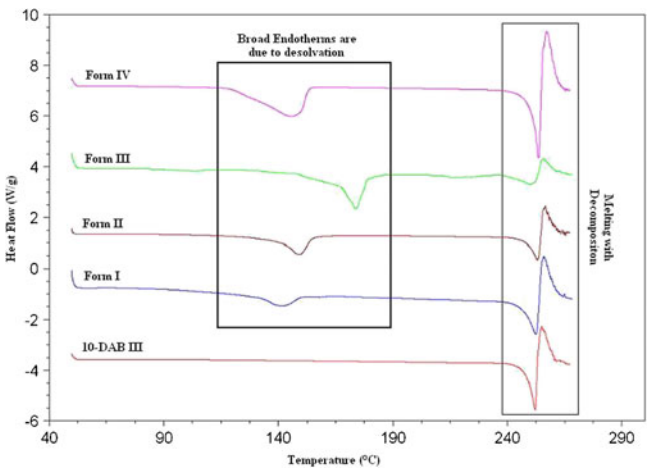

Fig. 8. DSC thermograms of 10-DAB III and its solid forms

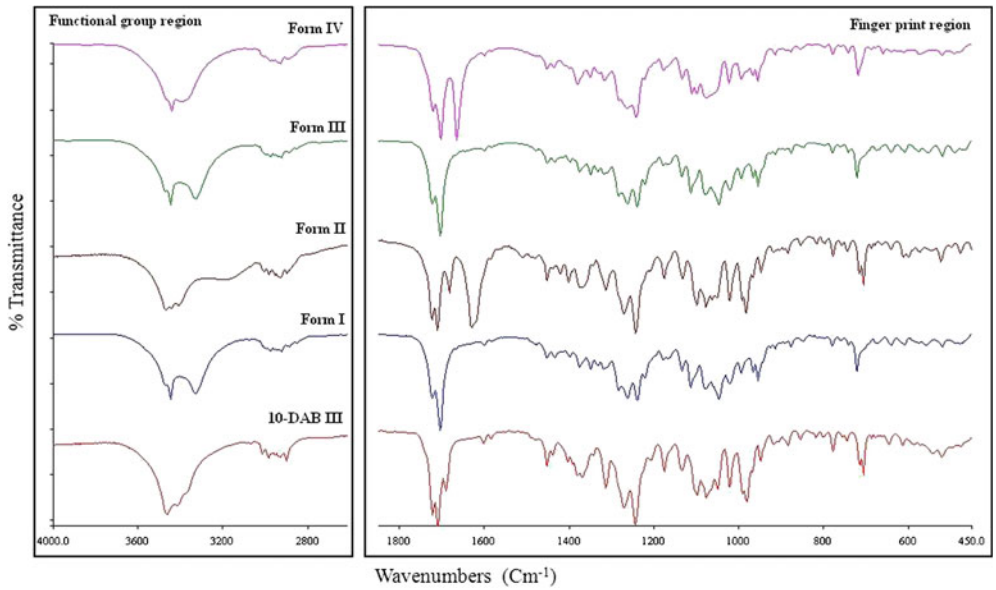

Fig. 9. FT-IR spectra of 10-DAB III and its solid forms

different solid-state forms of organic compounds. The shift and splitting pattern of absorption bands in FT-IR spectrum usually indicate a change in force constant, corresponding to a change in the environment of the corresponding bond, such as the bond length and bond angle. Figure 9 shows the FT-IR spectra of 10-DAB III and its solvates (Forms **I** to **IV**). The spectra of 10-DAB III and its solvates display clear differences in the region 3,600–3,300 (–OH stretching) cm^{-1} and 1,724–1,682 (C=O) cm^{-1}. The FT-IR spectra of both Forms **I** and **IV** demonstrate two C=O stretching frequencies apart from an amide C=O stretching. In case of 10-DAB III, Forms **II** and **III,** three C=O stretching frequencies are observed which could be due to the formation intramolecular hydrogen bond between C=O and the adjacent hydroxyl group. The amide C=O stretching frequencies at 1,667 and 1,630 $cm^{-1}$are observed in Forms **II** and **IV** solid forms and stretching frequencies resulting from S=O are observed at 1,048 and 1,019 cm^{-1} in Forms **I** and **III** solvates. These stretching frequencies indicate that the solvent molecules are occluded in the crystal lattices. The observed wavenumbers are tabulated in Table IV.

Table IV. Characteristic IR Bands of 10-DAB III and its Solid Forms

Compound	–OH stretching frequency	C=O stretching frequencies
10-DAB III	3466	1723[b], 1711[b], 1691[a]
Form **I**	3448, 3331	1724[b], 1705[b]
Form **II**	3442, 3396	1722[b], 1703[b], 1667[c]
Form **III**	3550, 3412, 3280	1725[b], 1708[b], 1682[a]
Form **IV**	3470, 3401	1724[b], 1712[b], 1683[a], 1630[c]

[a] Week stretching vibration
[b] Strong stretching vibration
[c] Amide C=O stretching

^{13}C SSNMR

In ^{13}C SSNMR spectroscopy, the chemical shifts are influenced by molecular packing, molecular conformation, molecular mobility, molecular structure and other solid-state effects. This method can be quite useful in developing an understanding of structural differences between different polymorphs or pseudopolymorphs (27,28). The differences in SSNMR carbon chemical shifts have been exploited by researchers to identify and quantify different polymorphs in mixture which are formed concomitantly (29).

^{13}C SSNMR spectra of 10-DAB III and its solid forms are shown in Fig. 10. The peak assignments based on liquid state ^{13}C NMR spectroscopy are presented in Table V. As expected, the spectra of 10-DAB III and its solid forms (Forms **I** to **IV**) exhibited significant differences in their chemical shifts. In 10-DAB III, Forms **I**, **II**, **III**, and **IV** the carbonyl carbon C9 assigned to the resonance at 211.72, 210.15, 214.36, 215.33, and 210.38 ppm, respectively. In case of Forms **II** and **III** the carbonyl carbon C9 assigned to the resonance farthest downfield when compared to the other forms, which could be due to the formation of intra and intermolecular hydrogen bonding. On the other hand, in 10-DAB III, Forms **I** and **IV** the carbonyl carbon C9 does not participate in any hydrogen bonding which was also confirmed by the solution state ^{13}C NMR data. In Forms **I** and **III**, the phenyl ring carbon atoms are expected to have typically four sets of signals but exhibited six different types of signals one from each carbon which is due to the differences in their torsion angles. The resonances of C2, C5, C9, C11, C12, C20, C21, and C23 are relatively well separated from those of other carbons; the chemical shifts of these carbons are chosen to distinguish the different morphs. The phenyl ring carbons (C24–C29) are assigned to the peaks between 127 and 135 ppm. For CH_3, CH_2, aliphatic CH and aliphatic

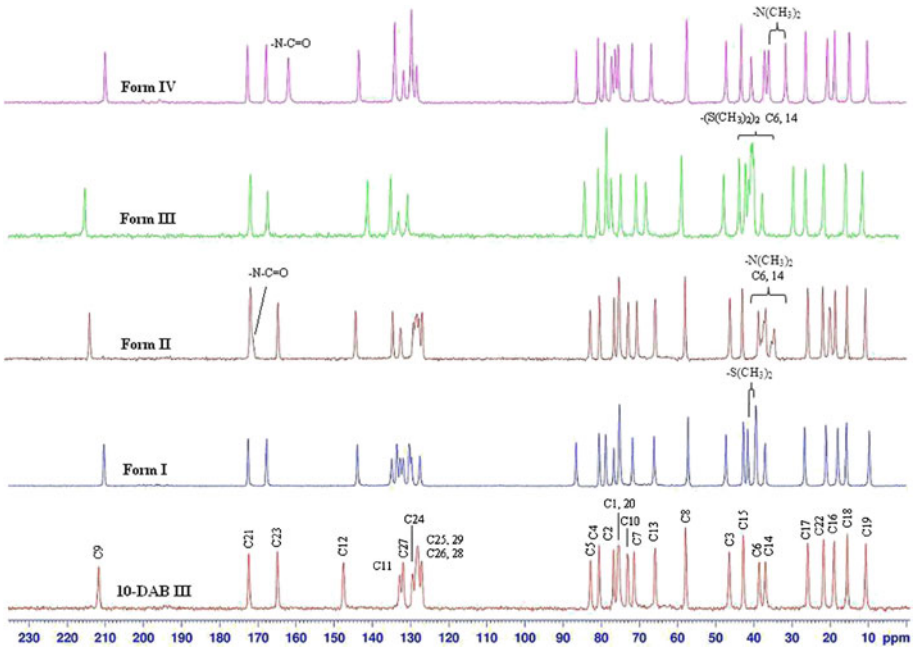

Fig. 10. Carbon-13 CPMAS spectra of 10-DAB III and its solid forms

quaternary carbons are assigned below 86.00 ppm. The peaks for other forms can be assigned similarly.

The peaks resulting from solvents are clearly demarcated at δ 39.33 and 41.51 ppm in Form **I**; 20.05, 34.72,

Table V. SS NMR^{13}C Chemical Shifts (δ/ppm) for 10-DAB III, Forms **I** to **IV** and Solution State of 10-DAB III

	Solution state	Solid state				
Carbon atom	10-DAB III	10-DAB III	I	II	III	IV
1	77.31	76.80	78.76	76.77	78.08	79.15
2	75.23	75.41	76.64	75.48	76.87	76.36
3	46.90	46.46	47.21	46.33	47.21	47.17
4	80.47	80.63	80.49	80.59	80.33	80.83
5	84.13	82.83	86.49	83.01	83.87	86.54
6	39.84	38.59	39.33	38.85	39.27	40.57
7	71.29	71.40	71.73	70.70	70.30	71.93
8	57.42	57.86	57.12	58.06	58.27	57.50
9	210.68	211.72	210.15	214.36	215.53	210.38
10	74.74	73.12	75.14	73.05	74.42	75.54
11	134.86	132.83	133.48	134.83	134.93	131.99
12	141.92	147.58	143.83	144.55	140.98	143.74
13	66.44	65.85	66.02	65.90	67.69	66.85
14	36.94	36.97	36.96	36.98	37.03	37.07
15	42.83	42.76	42.64	43.10	43.12	43.19
16	20.53	18.90	17.86	18.65	20.80	18.56
17	27.13	25.91	26.63	25.94	28.88	26.28
18	15.15	15.49	15.58	15.61	15.04	14.72
19	10.07	10.60	9.63	10.78	10.58	10.05
20	75.84	75.41	75.14	75.48	78.08	77.26
21	169.88	172.43	172.45	172.17	171.90	173.03
22	22.66	21.70	20.94	21.92	25.67	20.49
23	165.61	164.85	167.61	164.88	167.36	168.09
24	130.69	129.48	127.46	127.13	130.47	128.53
25	129.87	128.14	134.84	129.36	134.93	134.29
29			132.64	128.79		
26	129.01	127.12	131.86	128.47	132.87	129.88
28			129.67	127.95		
27	133.53	131.97	130.22	132.74		129.88

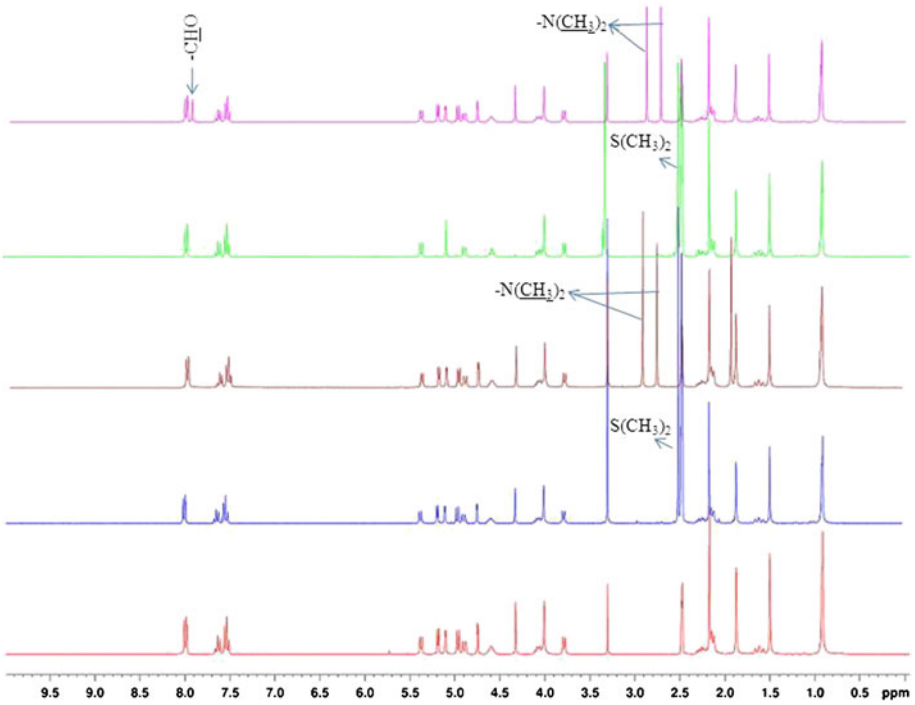

Fig. 11. ^{1}H NMR spectra of 10-DAB III and its solid forms

35.40, 37.42, 38.15 and 171.63 ppm in **II**; 39.65, 40.00, 40.61 and 41.45 ppm in **III** and 31.53, 35.99 and 162.19 ppm in **IV**. In Form **II**, the nitrogen attached carbon atoms ($(CH_3)_2$) resonates four peaks instead of two with an approximate equal intensity due to coupling to ^{14}N. Further, in Form **III,** four carbon signals are observed due to the presence of two molecules of DMSO located in different environments in the crystal packing system. Thus, the SSNMR provides valuable information for confirming the type of occluded solvent.

^{1}H NMR

^{1}H-NMR spectra (Fig. 11) were recorded in order to quantify the molecular proportions of solvate present in the solid-state forms of 10-DAB III. The stoichiometric ratios of solvents assessed by ^{1}H NMR experiments are consistent with the weight loss measurements observed by TGA and also concord with the theoretical values (Table VI).

Table VI. Quantitative Analysis Results from Solution-State NMR Experiments of 10-DAB III Solvates

Compound	Chemical shift, δ_H/ppm	Assignment	Molar ratio solvent: docetaxel
Form **I**	2.514	$(CH_3)_2$	1.01
Form **II**	2.917	CH_3	0.96
	2.760	CH_3	
Form **III**	2.514	$2(CH_3)_2$	2.07
Form **IV**	2.863	CH_3	0.97
	2.784	CH_3	
	7.925	CHO	

CONCLUSIONS

Pseudopolymorphs of 10-DAB III namely mono-DMSO (Form **I**), di-DMSO (Form **III**), mono-DMA (Form **II**), and mono-DMF (Form **IV**) were prepared by crystallization experiments. Crystallization of 10-DAB III from a single solvent (DMSO) resulted in formation of concomitant solvates mono-DMSO, di-DMSO, and crystallization in a binary mixture of solvents (DMSO/DMA, 1:1) resulted in formation of mono-DMA and di-DMSO solvates. Mono-DMF solvate was obtained by the crystallization of 10-DAB III in DMF solvent. All these four solvates are fully characterized by X-ray diffraction, thermal analysis, and spectroscopic techniques. Significant differences observed in the PXRD patterns of all the solid forms indicate the formation of distinct solid forms. From the thermal analysis, the author could confirm that the solvates, Forms **I**, **II** and **IV**, are having stoichiometric ratio of 1:1. But in case of Form **III**, the composition of 10-DAB III with DMSO solvent is found to be 1:2 stoichiometric ratio. The spectroscopic features of these solvates have been examined using FT-IR and SS ^{13}C NMR. In all the three crystal structures of Forms **I**, **II,** and **III** molecules form a host framework and the solvent molecules form the guest framework. From the above experimental data, it can be stated that the hydroxyl moieties (acceptor) of 10-DAB III are involved in hydrogen bonding with the donor solvent molecules and hence it can be concluded that 10-DAB III forms pseudopolymorphs with different solvents. In summary, we have highlighted the rare occurrence of the formation of two different stoichiometric solvates concomitantly from a single solvent and also from a binary mixture of solvents.

ACKNOWLEDGMENTS

We are grateful to the management of Aptuit Laurus Pvt. Ltd., for their encouragement and support to this research. We

thank Dr. Naba Kamal Nath for single-crystal structure refinement.

REFERENCES

1. Hagan M. Clathrate inclusion compounds. New York: Reinhold; 1962.
2. Lehn J-M. Supramolecular chemistry. Weinheim: VCH; 1995.
3. Desiraju GR. Crystal engineering: the design of organic solids. Amsterdam: Elsevier; 1989.
4. Weber E. Shape and symmetry in the design of new hosts. In: MacNicol DD, Toda F, Bishop R, editors. Comprehensive supramolecular chemistry, vol. 6. Oxford: Pergamon; 1996. p. 535–92. Chapter 17.
5. Weber E. Scissor-type hosts: molecular design and inclusion behaviour. In: Atwood JL, Davies JED, MacNicol DD, editors. Inclusion compounds, vol. 4. Oxford: Oxford University Press; 1991. p. 188–262. Chapter 5.
6. Nangia A. Organic host–guest structures in the solid-state. In: Lu GQ, Zhao XS, editors. Nanoporous materials: science and engineering. London: Imperial College Press; 2004. p. 165–87.
7. Bishop R. Designing new lattice inclusion hosts. Chem Soc Rev. 1996;25:311–9.
8. MacNicol DD, Downing GA. Symmetry in the evolution of host design. In: MacNicol DD, Toda F, Bishop R, editors. Comprehensive supramolecular chemistry, vol. 6. Oxford: Pergamon; 1996. p. 421–64.
9. Sumarna O, Seidel J. Crystal structure, thermal decomposition behavior, and order-disordertransition of the guest component of concomitant pseudodimorphic clathrates between 2,2′-bis(9-hydrozy-9-fluorenyl)biphenyl host and chloroform guest, 2003. Cryst Growth Des. 2003;3(4):541–6.
10. Ashmore J, Bishop R, Craig DC, Scudder ML. Comparison of the X-ray structures of concomitant pseudodimorphs formed between diquinoline host and *d*-chloroform guest. Mendeleev Commun. 2003;13:144.
11. Fabbiani FPA, Byrne LT, McKinnon JJ, Spackman MA. Solvent inclusion in the structural voids of Form II carbamazepine: single-crystal X-ray diffraction, NMR spectroscopy and Hirshfeld surface analysis. CrystEngComm. 2007;9:728–31.
12. Banerjee R, Bhatt PM, Desiraju GR. Solvates of sildenafil saccharinate. A new host material. Cryst Growth Des. 2006;6 (6):1468–78.
13. Sarma B, Nangia A. Tetrakis(4-sulfophenyl)methane didecahydrate. Reversible and selective water inclusion and release in an organic host. CrystEngComm. 2007;9:628–31.
14. Organo VG, Rudkevich DM. Emerging host–guest chemistry of synthetic nanotubes. Chem Commun. 2007;38:3891–9.
15. Sarma RJ, Baruah JB. Supramolecular and host–guest chemistry of bis-phenol and analogues. Cryst Growth Des. 2007;7(5):989–1000.
16. Jacobs A, Roex T, Nassimbeni LR, Toda F. Inclusion of volatile guests by a tetrapedal host: structure and kinetics. Org Biomol Chem. 2006;4(12):2452–7.
17. Cabeza AJC, Day GM, Motherwell WDS, Jones W. Solvent inclusion in Form II of carbamazepine. Chem Commun. 2007;1600–1602. doi:10.1039/b701299c.
18. Burchell TJ, Soldatov DV, Enright GD, Ripmeester JA. The ability of lower peptides to form co-crystals: inclusion compounds of Leu-Leu-Leutripeptide with pyridine and picolines. CrystEngComm. 2007;9:922–9.
19. Dalrymple SA, Shimizu GKH. Selective guest inclusion in a non-porous H-bonded host. Chem Commun. 2006;9:956–8.
20. Atwood JL, Barbour LJ, Jerga A. Storage of methane and freon by interstitial van der Waals confinement. Science. 2002;296(5577):2367–9.
21. Bernstein J, Davey RJ, Henck JO. Polymorphism in pharmaceutical industry. Angew Chem Int Ed. 1999;38:3440–61.
22. Das D, Barbour LJ. Concomitant formation of two different solvates of a hexa-host form a binary mixture of solvents. ChemCommun. 2008;5110–5112.
23. le Roux T, Nassimbeni LR, Weber E. Clathrates with mixed guests. Chem. Commun. 2007;1124–1126.
24. le Roux T, Nassimbeni LR, Weber E. Selectivity and structure of mixed guest clathrates. New J Chem. 2008;32:856–63.
25. Harper JK, Dalley NK, Mulgrew AE, West FG, Grant DM. 10-Deacetyl baccatin III dimethyl sulfoxidedesolvate. Acta Cryst. 2001;C57:64–5.
26. Dolomanov OV, Blake AJ, Champness NR, Schröder M. J Appl Cryst. 2003;3:1283.
27. Brittain HG. Physical characterization of pharmaceutical solids. New York, NY: Marcel Dekker; 1995.
28. Padden BE, Zell MT, Dong Z, Schroeder SA, Grant DJW, Munson EJ. Anal Chem. 1999;71:3325–31.
29. Vickery RD, Nemeth GA, Maurin MB. J Pharmaceut Biomed Anal. 2002;30:125–9.